

## A FOREGROUND CLEANED CMB MAP FROM NON-GAUSSIANITY MEASUREMENT

RAJIB SAHA<sup>1</sup>  
 Draft version July 17, 2021

### ABSTRACT

In this paper we present a new method to estimate a foreground cleaned Cosmic Microwave Background (CMB) map at a resolution of  $1^\circ$  by minimizing the non-Gaussian properties of the cleaned map which arise dominantly due to diffuse foreground emission components from the Milky Way. We employ simple kurtosis statistic as the measure of non-Gaussian properties and perform a linear combination of 5 frequency maps provided by Wilkinson Microwave Anisotropy Probe (WMAP) in its 7 year data release in such a way that the cleaned map has a minimum kurtosis which leads to a non-Gaussianity minimized, foreground cleaned CMB map. We validate the method by performing Monte-Carlo simulations. To minimize any residual foreground contamination from the cleaned map we flag out region near the galactic plane based upon results from simulations. Outside the masked region our new estimate of CMB map matches well with the WMAP's ILC map. A simple pseudo- $C_l$  based CMB TT power spectrum derived from the non-gaussianity minimized map reproduces the earlier results of WMAP's power spectrum. *An important advantage of the method is that it does not introduce any negative bias in angular power spectrum in low multipole regime, unlike usual ILC method.* Comparing our results with the previously published results we argue that CMB results are robust with respect to specific foreground removal algorithms employed.

*Subject headings:* cosmic background radiation — cosmology: observations — diffuse radiation

### 1. INTRODUCTION

The Cosmic Microwave Background (CMB) has conceivably become the finest tool so far to probe the physics of the early universe. The problem of isolating a clean CMB signal from contaminations originating from Milky Way is of primary importance to a cosmologist. According to the slowly rolling single scalar field inflationary scenario the primordial perturbations follow Gaussianity to a very good approximation, any non Gaussian properties predicted to be a small effect (Allen et al. (1987); Falk et al. (1992); Gangui et al. (1994); Acquaviva et al. (2003); Maldacena (2003)). Since CMB anisotropies are directly related to these perturbations via the spacetime metric one expects CMB to follow Gaussian distribution. It was shown by Munshi et al. (1995) that non-Gaussian effect introduced in CMB after decoupling is also small. It has been shown by Komatsu et al. (2003) that CMB data observed by WMAP satellite (Bennett et al. (1997)) is consistent with primordial Gaussian fluctuation. Contrary to these, diffuse foreground components, originating from our own galaxy exhibit highly non-Gaussian properties due to non-linearities involved in the physical processes during their origin. Based upon simple assumption of pure Gaussian properties of CMB and non-Gaussian nature of diffuse foregrounds, in this paper, we propose a new foreground removal method from CMB maps. A detailed account on several other foreground removal methods may be found in existing literatures (Brandt et al. (1994); Tegmark & Efstathiou (1996); Bouchet & Gispert (1999); Bennett et al. (2003); Tegmark et al. (2003); Saha et al. (2006); Hansen et al. (2006); Eriksen et al. (2006); Hinshaw et al. (2007); Saha et al. (2008); Eriksen et al. (2008b,a); Leach et al. (2008); Delabrouille et al. (2009); Samal et al. (2010); Pietrobon et al. (2010)). For discussions about searching for non-Gaussianity in foreground minimized CMB maps we refer to Räth et al. (2009); Barreiro et al. (2000); Banday et al. (2000); Raeth et al. (2010); Hou et al. (2010); Bernui & Rebouças (2010)).

### 2. METHODOLOGY

#### 2.1. Estimator for non-Gaussianity

A measure of non-Gaussian properties inherent in a collection of  $N$  random samples is given by so called kurtosis statistic, ( $\mathcal{K}$ ). For a set,  $S$ , of  $N$  random samples,  $S = \{x_i | i = 1, 2, 3, \dots, N\}$ , the  $\mathcal{K}$  statistic is defined as,

$$\mathcal{K} = \frac{1}{N} \sum_{i=1}^{i=N} \frac{(x_i - x_0)^4}{\sigma^4} - 3, \quad (1)$$

where  $x_0$  denotes sample mean and  $\sigma$  is the standard deviation of samples.  $\mathcal{K} = 0$  for samples drawn from Gaussian distribution whereas as discussed in Section 3.1 foreground distributions possess large positive kurtosis.

#### 2.2. Foreground Cleaned Map

Let  $\mathbf{X}_f$  denotes foreground contaminated CMB map in thermodynamic temperature unit at  $1^\circ$  resolution at a frequency index  $f$  and  $n_b$  represents total number of available frequency bands.  $\mathbf{X}_f$  is a column vector of  $n$  numbers where  $n$  is the number of surviving pixels at a frequency band after masking the known point source positions. We form a foreground cleaned map following,

$$\mathbf{X}^c = \sum_{f=1}^{n_b} w_f \mathbf{X}_f, \quad (2)$$

where  $w_f$  denotes the weight factor for linear combination for frequency index  $f$ . We choose these factors such that  $\mathcal{K}$  value for  $\mathbf{X}^c$  is minimized with an imposed constraint on them that  $\sum_{f=1}^{n_b} w_f = 1$ . This condition preserves the actual values of CMB temperature at each pixel in the foreground cleaned map.

Using Eqns. 1 and 2 one can show that,  $\mathcal{K}^c(\mathbf{W})$ , of the linearly combined map follows,

$$\mathcal{K}^c(\mathbf{W}) = \left[ \frac{n}{(\mathbf{W}\mathbf{T}\mathbf{W}^T)^2} \sum_{i=1}^n (\mathbf{W}\mathbf{T}_i\mathbf{W}^T)^2 \right] - 3, \quad (3)$$

where  $\mathbf{W}$  denotes a  $1 \times n_b$  vector whose  $f^{\text{th}}$  entry is given by  $w_f$  and  $\mathbf{T} = \sum_{j=1}^n \mathbf{T}_j$ . Here  $\mathbf{T}_j$  is a  $n_b \times n_b$  symmetric matrix for

<sup>1</sup> Physics Department, Indian Institute of Science Education and Research Bhopal, Bhopal, M.P, 462023, India.

pixel  $j$ ,  $\mathbf{T}_{j(ff')} = \Delta\bar{T}_{fj}\Delta\bar{T}_{f'j}$  where  $\Delta\bar{T}_{fj}$  denotes the temperature at pixel  $j$  of frequency index  $f$  after the mean temperature corresponding to this frequency has been subtracted from actual pixel temperature.

In principle, the solution for  $\mathbf{W}$  for minimum  $\mathcal{K}^c(\mathbf{W})$  satisfying our conditions can be obtained by employing a Lagrange's undetermined multiplier approach. However, because of non-trivial nature of dependency of  $\mathcal{K}^c$  on  $\mathbf{W}$  we find that such an approach is not feasible for our problem. Instead, we find the minimum of  $\mathcal{K}^c(\mathbf{W})$  by invoking a non-linear search algorithm due to Powell.

### 3. RESULTS

#### 3.1. Kurtosis

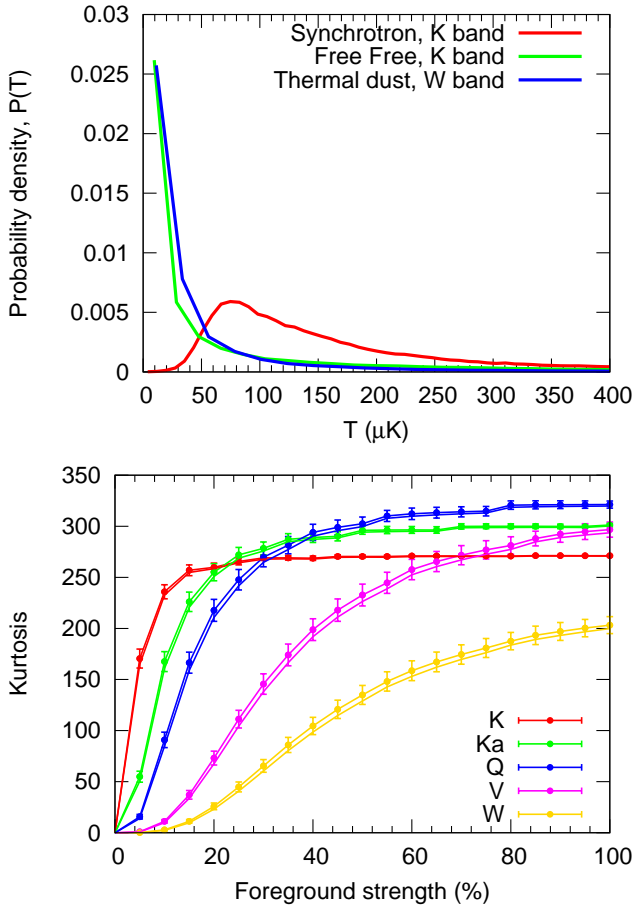


FIG. 1.— *Top Panel:* Non-Gaussian distribution of pixel temperature of MEM foreground maps. The frequency bands for this plots are chosen such that respective foreground component is most dominant over other frequencies inside the WMAP window. *Bottom Panel:* The plot of variation of kurtosis,  $\mathcal{K}$ , as a function of foreground strength at WMAP frequencies. The solid lines show mean curves obtained from the 150 random simulations of CMB and foreground with foreground strength as indicated by the ordinate of each point. The dashed lines show the variation of kurtosis for a randomly chosen realization. The error bars indicate cosmic variance. Mean kurtosis estimated from pure CMB maps is given by,  $\langle\mathcal{K}_{CMB}\rangle = -0.023 \pm 0.060$ .

The distributions of pixel temperatures due to diffuse galactic foregrounds are shown in top panel of Fig. 1. Each of these foreground distributions is strongly asymmetric and exhibits a long tail towards positive temperature direction indicating a variation slower than  $\sim e^{-T^2}$ , which is the case for a Gaussian distribution. The peak for the synchrotron distribution shows

that at 23GHz most likely contamination due to synchrotron occurs at a temperature  $\sim 75\mu\text{K}$ , although contaminations at high ( $> 400\mu\text{K}$ ) and low (e.g., as low as  $< 25\mu\text{K}$ ) pixel temperature are also likely.

How does  $\mathcal{K}$  vary with foreground contamination in CMB maps at different WMAP frequencies? To answer this question we generate 150 random full sky CMB maps using WMAP's LCDM power spectrum. With each of these random realization of CMB map we add WMAP's MEM foreground templates at various strengths. The resulting behavior of the  $\mathcal{K}$  with foreground strength is shown in Fig. 1 for all WMAP frequency bands. For each band  $\mathcal{K}$  increases as the amount of foreground contamination increases. For K band the variation takes a shape of a plateau, characterized by a slow increase of  $\mathcal{K}$ , as the foreground level reaches  $\sim 20\%$  of its full level. For all bands  $\mathcal{K}$  becomes more than 150 when all foregrounds are operative at their 100% level. It is interesting to note that the Q band (not the K band which has the highest level of synchrotron and free free contamination) shows the largest  $\mathcal{K}$  value among all the 5 bands at the maximum foreground strength.

#### 3.2. Validation of the Method

We validate the methodology by performing Monte-Carlo simulations. We use MEM foreground maps for synchrotron, free free and thermal dust available from LAMBDA website. These maps are provided in a common resolution of  $1^\circ$  and at pixel resolution parameter  $n_{\text{side}} = 256$  in antenna millikelvin temperature unit. We upgrade the pixel resolution of each map to  $n_{\text{side}} = 512$  and convert them to thermodynamic microkelvin unit. We add the composite foreground map of each WMAP frequency with a random realization of CMB compatible to LCDM model to make foreground contaminated CMB maps at each of the WMAP frequencies. Finally, we mask the position of the known point sources using the WMAP's 7 year point source mask.

We develop a C code (hereafter *GaussMap*) to implement constrained Powell's conjugate gradient method. We perform 200 Monte-Carlo simulations of foreground removal method. From these simulations we find that the foreground removal is effective over almost all parts of the sky. However, we find visible signature of some residual foreground emission in the inner plane of the galaxy. To find out the sky regions where the residual foreground could be significant compared to the expected CMB signal we subtract average of input CMB maps from the average of foreground cleaned maps. Then we form an initial mask by assigning zero values to all pixels with absolute temperature values more than  $20\mu\text{K}$  of this map and unity at all other pixels. This mask contains a set of scattered pixels in the inner galactic plane. To remove these pixels we first smooth the initial mask by a Gaussian window of  $1^\circ$ . We transform this smoothed mask to a new mask by assigning all pixels of smoothed mask with values greater than or equal to 0.9 to a new value of unity and the all other pixels to zero. To exclude position of the known point sources from the analysis we make the final mask multiplying this mask by the WMAP's point source mask. We call the resulting mask as G20 mask. This retains  $\sim 87\%$  of the entire sky area.

We estimate  $\mathcal{K}$  for each of the cleaned maps obtained from Monte-Carlo simulations of foreground removal procedure<sup>2</sup>. The mean kurtosis obtained from all the cleaned maps is given by  $\langle\mathcal{K}\rangle = 0.86 \pm 0.21$ . This corresponds to  $\sim 4\sigma$  detection of

<sup>2</sup> Note that the position of known point sources are excluded before computing the  $\mathcal{K}$  values.

non Gaussianity from the cleaned maps. We interpret the non-vanishing  $\langle K \rangle$  in terms of residual foreground contamination originating from the galactic plane. After flagging of the pixels determined by the G20 mask we obtain,  $\langle K \rangle = -0.02 \pm 0.06$ , which is consistent with zero. Henceforth, we use G20 mask as the basic mask to remove pixels contaminated by the residual foreground while analyzing cleaned maps from Monte-Carlo simulations as well as WMAP data. The mean weights for 5 frequency bands satisfy,  $\langle \mathbf{W} \rangle = (0.049 \pm 0.021, -0.419 \pm 0.063, -0.213 \pm 0.027, 1.643 \pm 0.063, -0.059 \pm 0.029)$ .

### 3.2.1. Temperature Distribution

Using the Monte-Carlo simulations we verify that the pixel temperature of cleaned maps outside the G20 mask follows a Gaussian distribution. For this we apply G20 mask both to a randomly chosen CMB realization and its foreground cleaned counterpart. To verify the Gaussian nature of these distributions we fit the histogram of input CMB map (after G20 mask is applied) by a normalized Gaussian probability distribution,  $g(T) = \exp(-(T-a)^2/(2s^2))/\sqrt{(2\pi s^2)}$ , where  $a$  and  $s$  denote respectively mean and standard deviation of the distribution. From the fit we find that,  $s = 69.95 \pm 0.09 \mu K$  and  $a = 2.12 \pm 0.11 \mu K^3$ .

### 3.2.2. Power Spectrum

We apply G20 mask on each of the 200 foreground cleaned CMB maps and estimate full sky estimate of CMB power spectrum using MASTER method (Hivon et al. (2002)). The average of 200 power spectra obtained from the foreground removed maps matches excellently with the average of the input CMB power spectra. We show both spectra in Fig. 2 along with the cosmic variance. This verifies that no significant foreground contamination exists outside the G20 mask and the method outlined in this paper can be used to estimate CMB power spectrum to extract cosmological information.

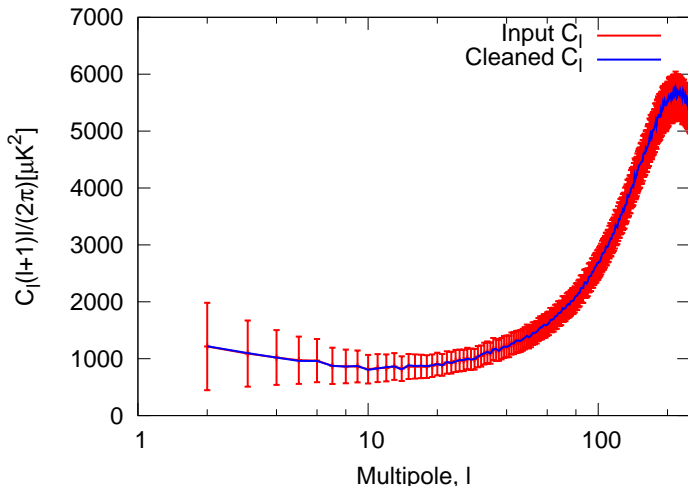


FIG. 2.— Comparison of average power spectrum obtained from foreground cleaned CMB maps outside G20 mask (red) with the average input CMB power spectrum, (red line with errorbars). The average cleaned power spectrum is obtained by using MASTER algorithm. Both spectra have beam and pixel window effects removed.

In some of the earlier publications (Saha et al. (2006); Souradeep et al. (2006); Saha et al. (2008); Samal et al. (2010)) the authors reported that the harmonic space based ILC method

<sup>3</sup> The small monopole is a manifestation of cosmic variance.

gives rise to a negative bias in its power spectrum at the low multipoles. The bias appears due to a mere chance correlation between CMB and foregrounds at large angles due to availability of only small number of modes in the large scales on the sky. In principle, the negative bias in the power spectrum can be present in both pixel based and multipole based ILC algorithms which rely upon minimization of net foreground variance from the cleaned map, since in these cases the finite correlation between CMB and foregrounds arises due to certain degree of overlap between hot spots and cold spots of CMB and foregrounds and the algorithm creates a negative bias due to nonlinear dependence of weights on the empirical covariance matrix (Saha et al. (2008)). However, the foreground removal method described in this paper relies upon the Gaussian nature of the final distribution, without explicitly minimizing the variance of the data. This leads to the advantage that the power spectrum obtained from the cleaned map does not have any negative bias.

### 3.3. Application on WMAP data

Before the analysis we mask out the positions of known point sources from each of WMAP's 5 frequency maps using the point source mask. After masking each map contains 3054273 pixels comprising 97% of the full sky area.

#### 3.3.1. Non-Gaussianity minimized map

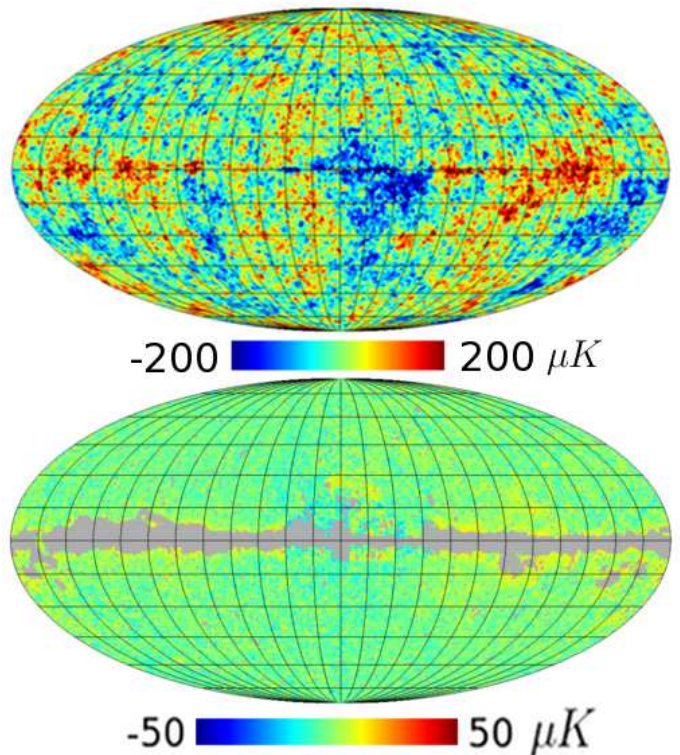


FIG. 3.— *Top panel:* The foreground removed GMAP obtained by minimizing  $K^c(\mathbf{W})$ . The map has a beam resolution of  $1^\circ$  and a pixel resolution corresponding to pixel resolution parameter  $n_{side} = 512$ . *Bottom panel:* The difference between GMAP and the WMAP's 7 year's ILC map outside G20 mask.

We use *GaussMap* code to estimate the best fit weight factors corresponding to different frequency bands. The code gives best choice of weights as  $\mathbf{W} = (0.035, -0.378, -0.217, 1.632, -0.073)$  for K to W bands corresponding to  $K_{min}^c(\mathbf{W}) = 1.17$ . The complete procedure to



estimate the weights takes only about a couple of minutes on an Intel 2.26 GHz processor. As one might expect, V band gets the maximum positive weight since it is supposed to be the least foreground contaminated frequency band in the WMAP observation window. The kurtosis for cleaned map outside the G20 mask becomes 0.093. We note that weights obtained from WMAP data have similar values to the mean weights obtained from Monte-Carlo simulations in Section 3.2.

Using the weights described above we obtain the foreground cleaned CMB map (top panel of Fig. 3, hereafter GMAP). Although there are some visible signature of presence of residual foreground contamination in this map on the galactic plane (e.g. Cygnus region, Cassiopeia A, Carina nebula) all contaminations are confined only near the galactic plane. We show the difference between GMAP and WMAP's 7 year ILC map outside the G20 mask in bottom panel of Fig. 3. In the unmasked difference map larger pixel amplitudes are confined near the galactic plane, making a narrow strip-like structure, with absolute pixel temperature exceeding  $50\mu K$ . The bottom panel of Fig. 3 shows that applying G20 mask significantly reduces pixel amplitude of the difference map..

### 3.3.2. Temperature Distribution

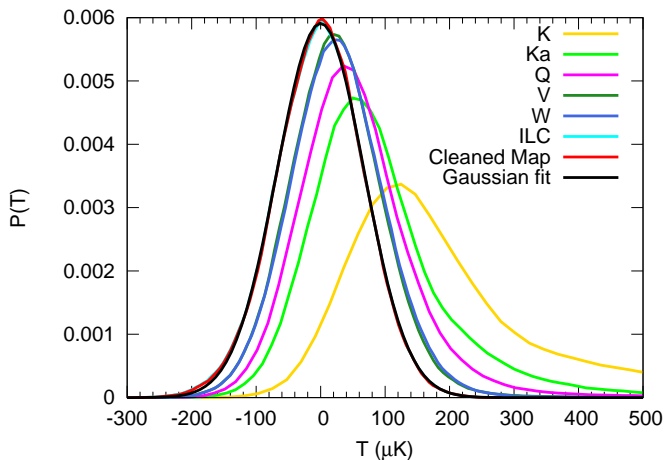


FIG. 4.— The distribution of the pixel temperatures of GMAP outside G20 mask is shown in red. The black curve shows a Gaussian fit to this data. The cyan curve shows the distribution of ILC map outside G20 mask. The other curves show the non-Gaussian distributions of pixel temperatures outside G20 mask for each of the individual WMAP frequency band. Note that since these frequency maps contain CMB their distributions extend to negative pixel values.

We test for the distribution of pixel temperature of GMAP outside the G20 mask. The average pixel temperature of this map outside the G20 mask is only  $0.85\mu K$ . Hence we fit for a Gaussian probability function with mean 0 and variance  $s$  to the pixel temperature distribution of the masked GMAP. From the fit we obtain,  $s = 67.49 \pm 0.12\mu K$ . We show the distribution outside G20 mask obtained from GMAP and the WMAP's ILC map in Fig. 4. We also show in this figure pixel temperature distributions of individual frequency bands. The long tails for K and Ka bands are due to strong synchrotron contamination. We note that all the distributions corresponding to 5 frequency bands are asymmetric representing their non-Gaussian nature. Pixel temperature of simulated frequency maps have distributions similar to these histograms.

### 3.3.3. Power Spectrum

To estimate power spectrum from GMAP we first apply G20 mask and estimate the partial sky CMB power spectrum. We convert the partial sky power spectrum to the full sky estimate by inverting the mode-mode coupling matrix. Finally we remove both beam and pixel effect from this power spectrum. We show the resulting power spectrum in Fig. 5. As shown in this figure this power spectrum matches well with the ILC power spectrum estimated from the same sky region until  $l \sim 100$ . Beyond this multipole range GMAP power spectrum has less power than the ILC power spectrum. From the GMAP we find  $C_2 = 246.4\mu K^2$  and  $C_3 = 402.3\mu K^2$  consistent with ILC estimates ( $C_2 = 248.8\mu K^2$  and  $C_3 = 404.0\mu K^2$ ).

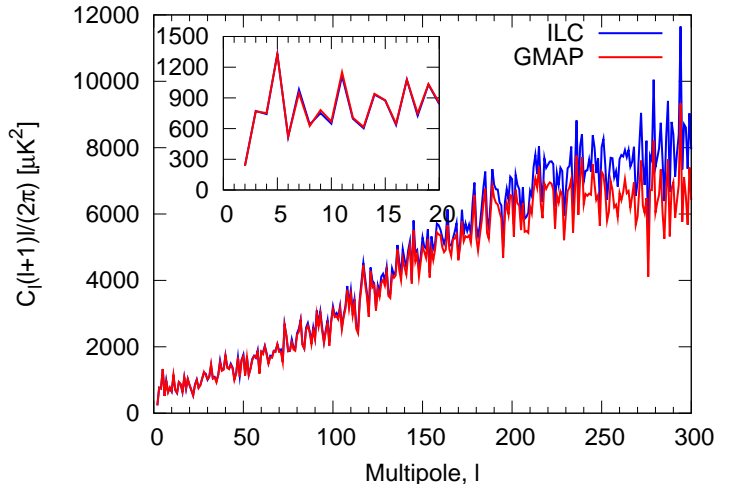


FIG. 5.— Full sky estimate of CMB Power spectrum from GMAP outside the G20 mask is shown in red line. The full sky estimate of WMAP's ILC power spectrum computed from the same region is shown in blue line. Both spectra have been corrected for  $1^\circ$  beam effect and pixel window effect. In the inset we zoom in low multipole region. Both spectra match excellently with one another until  $l \sim 100$ .

## 4. DISCUSSIONS & CONCLUSION

In this paper we have developed, validated and applied on 7 year WMAP data a global foreground minimization method from CMB sky based upon the measure of non-Gaussian nature of the diffuse galactic foregrounds. The GMAP obtained by this method matches well with the WMAP's ILC map outside the G20 mask. The power spectrum from GMAP also matches excellently with the power spectrum of ILC map until  $l \sim 100$ . At even higher  $l$  we find less power than WMAP's ILC map. The kurtosis value of the foreground minimized map outside the G20 mask,  $0.093 \pm 0.06$ , the error is estimated from Monte-Carlo simulations of foreground removal method. This is only a  $1.5\sigma$  effect implying that the CMB sky outside the G20 region is sufficiently clean so that the signals from this region may be interpreted to have cosmological origin consistent with standard cosmological scenario.

A crucial advantage of the method over the usual variance based ILC method is that the former does not possess any negative bias at low multipoles. The quadrupole moment estimated by us matches excellently with the WMAP's ILC estimate. Our result shows that the problem of low quadrupole moment persist in WMAP data. The quadrupole and octopole maps also show similar nature as the ones estimated from the WMAP's ILC map. The problem of quadrupole and octopole alignment using GMAP would be investigated in a future paper - however, given the similarity between GMAP and ILC map (at the least, outside the G20 mask) the alignment likely

to remain. Another direction for future research would be to implement the method in the harmonic domain of the maps. The method can be generalized to estimate CMB angular power spectrum down to low angular scale following approaches described in Saha et al. (2006) and Saha et al. (2008). Since polarized foreground models are poorly known, an excellent research direction would be to apply our method on polarization sensitive CMB data released by WMAP and PLANCK satellite mission (Tauber (2001)).

Our method shows that it is possible to remove foregrounds from the CMB sky purely based upon non-Gaussian nature of non-cosmological signals. However, if there is any cosmological signal of non-Gaussian origin the method would interpret them as *foregrounds* and hence would try to eliminate the sig-

nal from the cleaned map. Therefore comparing the GMAP with other foreground minimized maps which do not explicitly rely upon the assumption of non-Gaussianity one may be able to isolate any possible primordial and/or secondary non-Gaussian signal. Estimating a Gaussian CMB map using data from current and future generation sensitive CMB experiments like PLANCK and CMBPol would play an important role to unfold this scientific information.

We thankfully acknowledge useful discussions with Tarun Souradeep and Jayanta Kumar Bhattacharjee. Some of the results of this paper are obtained by using HEALPix software package (Górski et al. 2005)<sup>4</sup>. We acknowledge use of LAMBDA data repository for our analysis.

## REFERENCES

- Acquaviva, V., Bartolo, N., Matarrese, S., & Riotto, A. 2003, Nuclear Physics B, 667, 119
- Allen, T. J., Grinstein, B., & Wise, M. B. 1987, Physics Letters B, 197, 66
- Banday, A. J., Zaroubi, S., & Górski, K. M. 2000, ApJ, 533, 575
- Barreiro, R. B., Hobson, M. P., Lasenby, A. N., Banday, A. J., Górski, K. M., & Hinshaw, G. 2000, MNRAS, 318, 475
- Bennett, C. L., et al. 1997, in Bulletin of the American Astronomical Society, Vol. 29, American Astronomical Society Meeting Abstracts, 1353–+
- Bennett, C. L., et al. 2003, ApJS, 148, 97
- Bernui, A., & Rebouças, M. J. 2010, Phys. Rev. D, 81, 063533
- Bouchet, F. R., & Gispert, R. 1999, New Astronomy, 4, 443
- Brandt, W. N., Lawrence, C. R., Readhead, A. C. S., Pakianathan, J. N., & Fiola, T. M. 1994, ApJ, 424, 1
- Delabrouille, J., Cardoso, J.-F., Le Jeune, M., Betoule, M., Fay, G., & Guillooux, F. 2009, A&A, 493, 835
- Eriksen, H. K., Dickinson, C., Jewell, J. B., Banday, A. J., Górski, K. M., & Lawrence, C. R. 2008a, ApJ, 672, L87
- Eriksen, H. K., Jewell, J. B., Dickinson, C., Banday, A. J., Górski, K. M., & Lawrence, C. R. 2008b, ApJ, 676, 10
- Eriksen, H. K., et al. 2006, ApJ, 641, 665
- Falk, T., Rangarajan, R., & Srednicki, M. 1992, Phys. Rev. D, 46, 4232
- Gangui, A., Lucchin, F., Matarrese, S., & Mollerach, S. 1994, ApJ, 430, 447
- Górski, K. M., Hivon, E., Banday, A. J., Wandelt, B. D., Hansen, F. K., Reinecke, M., & Bartelmann, M. 2005, ApJ, 622, 759
- Hansen, F. K., Banday, A. J., Eriksen, H. K., Górski, K. M., & Lilje, P. B. 2006, ApJ, 648, 784
- Hinshaw, G., et al. 2007, ApJS, 170, 288
- Hivon, E., Górski, K. M., Netterfield, C. B., Crill, B. P., Prunet, S., & Hansen, F. 2002, ApJ, 567, 2
- Hou, Z., Banday, A. J., Górski, K. M., Elsner, F., & Wandelt, B. D. 2010, MNRAS, 407, 2141
- Komatsu, E., et al. 2003, ApJS, 148, 119
- Leach, S. M., et al. 2008, A&A, 491, 597
- Maldacena, J. 2003, Journal of High Energy Physics, 5, 13
- Munshi, D., Souradeep, T., & Starobinsky, A. A. 1995, ApJ, 454, 552
- Pietrobon, D., Balbi, A., Cabella, P., & Gorski, K. M. 2010, ApJ, 723, 1
- Raeth, C., Banday, A. J., Rossmanith, G., Modest, H., Suetterlin, R., Gorski, K. M., Delabrouille, J., & Morfill, G. E. 2010, ArXiv e-prints
- Räth, C., Morfill, G. E., Rossmanith, G., Banday, A. J., & Górski, K. M. 2009, Physical Review Letters, 102, 131301
- Saha, R., Jain, P., & Souradeep, T. 2006, ApJ, 645, L89
- Saha, R., Prunet, S., Jain, P., & Souradeep, T. 2008, Phys. Rev. D, 78, 023003
- Samal, P. K., Saha, R., Delabrouille, J., Prunet, S., Jain, P., & Souradeep, T. 2010, ApJ, 714, 840
- Souradeep, T., Saha, R., & Jain, P. 2006, New A Rev., 50, 854
- Tauber, J. A. 2001, in IAU Symposium, Vol. 204, The Extragalactic Infrared Background and its Cosmological Implications, ed. M. Harwit & M. G. Hauser, 493–+
- Tegmark, M., de Oliveira-Costa, A., & Hamilton, A. J. 2003, Phys. Rev. D, 68, 123523
- Tegmark, M., & Efstathiou, G. 1996, MNRAS, 281, 1297

<sup>4</sup> The HEALPix distribution is publicly available from the website <http://healpix.jpl.nasa.gov>.